Resonant motion of discrete breathers in curved nonlinear chains

2001 J. Phys. A: Math. Gen. 34 8465

(http://iopscience.iop.org/0305-4470/34/41/305)

INSTITUTE OF PHYSICS PUBLISHING JOURNAL OF PHYSICS A: MATHEMATICAL AND GENERAL

J. Phys. A: Math. Gen. **34** (2001) 8465–8475 PII: S0305-4470(01)25092-6

Resonant motion of discrete breathers in curved nonlinear chains

R Reigada[1], **J M Sancho**[2], **M Ibañes**[2] **and G P Tsironis**[3]

[1] Departament de Química Física, Universitat de Barcelona, Avgda. Diagonal 647, Barcelona 08028, Spain
[2] Departament d'Estructura i Constituents de la Matèria, Universitat de Barcelona, Avgda. Diagonal 647, Barcelona 08028, Spain
[3] Department of Physics, University of Crete and Foundation for Research and Technology-Hellas, PO Box 2208, 71003 Heraklion, Crete Greece

Received 8 May 2001
Published 5 October 2001
Online at stacks.iop.org/JPhysA/34/8465

Abstract

We present the study of discrete breathers moving resonantly in a two-dimensional polymeric hairpin-shaped model with perpendicular onsite potentials. Their motion adapts to the local dynamical environment and move more efficiently in the curve in several cases. This motion is locally governed by conservation of energy. Weak dissipation and thermal noise do not affect these phenomena qualitatively.

PACS numbers: 05.45.−a, 02.60−x, 05.40.−a, 05.90.+m, 81.05.Lg

1. Introduction

Discrete breathers (DBs) or intrinsic localized modes (ILMs) are localized oscillations that can trap and transfer efficiently vibrational energy many times in discrete nonlinear lattice systems [1–9]. They are interesting theoretically since they act in a way similar to impurity modes in systems with translational invariance, and they are also interesting experimentally since they seem to arise naturally in diverse systems with high effective nonlinearity [10–13]. It has been conjectured that DBs can play an important role in energy storage and transfer in biomaterials such as proteins [9, 14]; as a result, the role of biopolymer geometry and its interplay with nonlinearity will be a decisive factor in efficient energy and mass transport across a biomolecule [15, 16]. Recent work in this direction has demonstrated that DBs can indeed be created in curved nonlinear lattice chains and can also propagate across polymer bends [17, 18]. In particular, in reference [18] it was demonstrated that if a standard Fermi–Pasta–Ulam (FPU) chain is constrained on an arbitrary planar curve and DBs are constructed in a rectilinear part of the chain, they can traverse a circularly curved part of the chain with a speed smaller than that of the injected one provided the penetration angle to the curve is not too large; in the opposite case they simply rebounce or get trapped. Even though this work shows basic features of

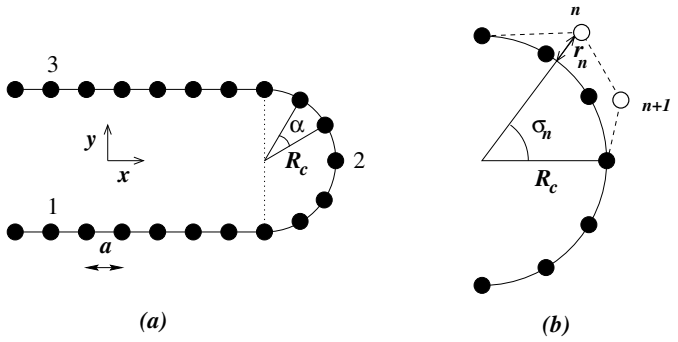

Figure 1. (*a*) Schematic representation of the equilibrium conformation for the hairpin. Black dots are the equilibrium positions of the particles in the hairpin for $N_c = 5$. The location labelled by 1 is a typical starting point for the breather, 2 denotes a point in the curve and 3 a final point. (*b*) White dots are the nonequilibrium position of the particles with their polar coordinates used in some of the figures below to represent the motion of the breather in the curved part of the hairpin.

DB dynamics in curved polymers, it does not address fully the two-dimensional case since it tackles constrained motion with fixed angles. In the present work, we lift this restriction and handle the complete two-dimensional dynamics of a polymeric chain in the shape of a hairpin, viz. that of two straight segments joined by a semicircle. In a biological context this shape can describe a β-sheet connection of a protein or a similar DNA configuration. Our model then consists of an FPU chain in the form of a hairpin that is confined via onsite potentials in the direction perpendicular to that of the hairpin; their role is to stabilize the chain that is naturally degenerate on the plane due to the inclusion of only first neighbour interactions [15, 16, 18]. The questions we would like to address revolve around the following points: (a) What are the kinetic properties of a DB launched in the rectilinear part of the chain towards the curved one? (b) How does the inclusion of the second dimension and the presence of the onsite potential affect the DB motion? (c) Is the motion dynamically stable at low ambient temperatures, i.e. under the simultaneous presence of Langevin noise and small damping? In section 2 we introduce our model and describe the numerical scheme, and in section 3 we present the main results and the answers to questions (a) and (b). In section 4 we study the DB dynamics under fluctuation–dissipation conditions, and finally in section 5 we conclude.

2. Model for the hairpin chain

The model presented in this paper is developed in Cartesian coordinates, using a nearest-neighbour interaction that follows the FPU potential for the distance between nearest nodes, $d_n = \left[(x_n - x_{n-1})^2 + (y_n - y_{n-1})^2\right]^{1/2}$, where (x_n, y_n) denote the absolute Cartesian coordinates of the nth mass m. This potential reads

$$V_d(d_n) = \tfrac{K}{2}(d_n - a)^2 + \tfrac{\beta}{4}(d_n - a)^4 \tag{1}$$

where K and β are the constants of the FPU model and a is the equilibrium separation between two adjacent sites of the chain. We also include a 'perpendicular-to-the-hairpin' onsite potential in order to keep the hairpin shape. The equilibrium hairpin conformation in Cartesian coordinates is shown in figure 1(a).

The perpendicular potential reads

$$V_p(r_n) = \tfrac{1}{2}K_2 r_n^2 + \tfrac{1}{4}K_3 r_n^4 \tag{2}$$

where r_n designates the radial distance to the equilibrium point in the semicircle (see figure 1(b)) or the vertical distance orthogonal to the equilibrium line in the rectilinear segment of the hairpin. With this potential, the chain always tries to recover the hairpin conformation, but it is not rigidly constrained to such a shape as it was in [18]. Moreover, the perpendicular potential avoids the generally unstable arbitrary motion on the plane [15, 16].

Considering both potentials we obtain the following Hamiltonian:

$$\mathcal{H} = \sum_n \left(\frac{\dot{x}_n^2}{2m} + \frac{\dot{y}_n^2}{2m} \right) + \sum_n \left[V_d(d_n) + V_p(r_n) \right]. \tag{3}$$

In our numerical simulations, a certain number of nodes are placed at the equilibrium positions, i.e. $r_n = 0$ and $d_n = a$, $\forall n$. This implies that the number of sites initially in the curved part of the chain, N_c, will determine the radius R_c and subsequently the curvature of the hairpin. As the equilibrium distance a is fixed, the relation between R_c and N_c follows from simple geometric calculations,

$$R_c = \frac{a}{2\sin\left(\frac{\pi}{2(N_c+1)}\right)}. \tag{4}$$

We generate numerically one-dimensional exact discrete breathers following the anticontinuous limit procedure [4] and place them along the longitudinal x-axis on the hairpin (close to point 1 of figure 1). Specifically, we use an initial breather with a period of $T_b \approx 2.1223$ from a single pulse in relative one-dimensional coordinates ($\rho_n \equiv x_n - x_{n-1} - a$). Since we are interested in energy transport properties, we need to induce the motion by giving some values to the initial velocities $\{\dot{\rho}_n(0)\}$. Using a simple approximation of the pinning mode excitation method [5], we initially kick the breather by assigning a proportion λ of the gradient of its absolute value, or velocity pinning mode vector $\{|\rho_n|'\}$,

$$\dot{\rho}_n(0) = \lambda |\rho_n|' \tag{5}$$

where spatial derivatives are taken to be symmetric. This translational motion, as it is defined, sends the breather from the sites near point 1 in figure 1 to the curved part of the chain. This approximate procedure for generating mobile DBs causes the detachment of a small portion of the initial breather energy that propagates away very fast with a localized phonon shape. The initial breather in relative coordinates, ρ_n, and velocities, $\dot{\rho}_n$, are shown in figure 2.

3. Numerical results

Numerical results are obtained by using a fourth-order Runge–Kutta method to solve the equations of motion (directly in Cartesian coordinates) that follow from equations (1)–(3). We fix some of the parameters that describe the model. For the equations of motion, we set $K = \beta = 1$ and $a = 3$. For the velocity parameter λ, a value of 0.8 is assigned. This value corresponds to a translational velocity of the breather (in the straight part of the chain) equal to 0.45 in our dimensionless units of space and time (the speed of sound has value 3 in these units). Moreover, in our simulations the total number of sites is larger than 1000, and as a result no phonon–breather interaction takes place during the simulation. The specific perpendicular potential parameters, i.e. (K_2, K_3), and the curvature of the hairpin fixed by the number of sites in the curved part of the chain, i.e. N_c, determine the different cases to be studied.

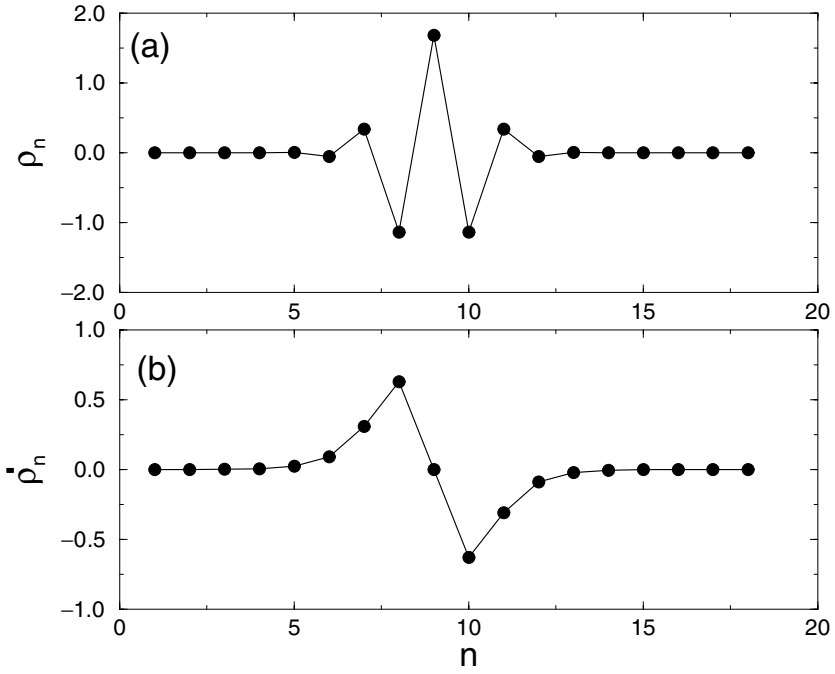

Figure 2. (*a*) The initial breather in relative coordinates. (*b*) The initial velocities (for $\lambda = 1$) also in relative coordinates.

The onsite perpendicular potential plays a central role in the breather dynamics since it is responsible for localized energy interchange and directional mixing in the curved part of the hairpin. Although in most of the cases the breather is found to be able to traverse the hairpin, there is some energy loss during the initial entry in the curve. This loss depends on the nature of the energy interchange between the radial and tangential DB direction in the bend that is also responsible for the specifics of the DB propagation through the bend. A suitable selection of the onsite potential parameters (K_2, K_3) minimizes the energy loss and permits the resonant motion of the breather through the bend. In order to check these ideas, we compare four different cases: two quadratic perpendicular potentials with $K_2 = 1$ and $K_2 = 8$ and two hard potentials with $K_2 = K_3 = 1$ and $K_2 = K_3 = 6$. In figure 3(*a*), we plot the period-versus-amplitude dependence of the individual potentials and note that only the anharmonic potential $K_2 = K_3 = 6$ and the harmonic case $K_2 = 8$, $K_3 = 0$ have a period very close to T_b.

It is clear from figure 3(*b*) that the breather adapts better in the anharmonic cases. For example, for the purely quadratic case with $K_2 = 8$, where the DB frequency almost coincides with the frequency of the perpendicular potential, the breather cannot traverse the hairpin. In some other cases with $K_3 = 0$, the breather is able to tranverse the hairpin but these appear to be exceptional situations and depend on the frequency shift of the DB relative to the harmonic frequency. Actually, the quadratic case with $K_2 = 1$ in figure 3 corresponds to one of these situations. Although a purely quadratic onsite potential does not allow by itself more than one single frequency for the perpendicular motion, the existence of nonlinearity in the interaction potential, $V_d(d_n)$, provides an alternative mechanism to traverse the hairpin which is not always effective, as we have seen in the case $K_2 = 8$. The presence of nonlinearity in the onsite perpendicular forces introduces frequency shifts that improve the resonance in the

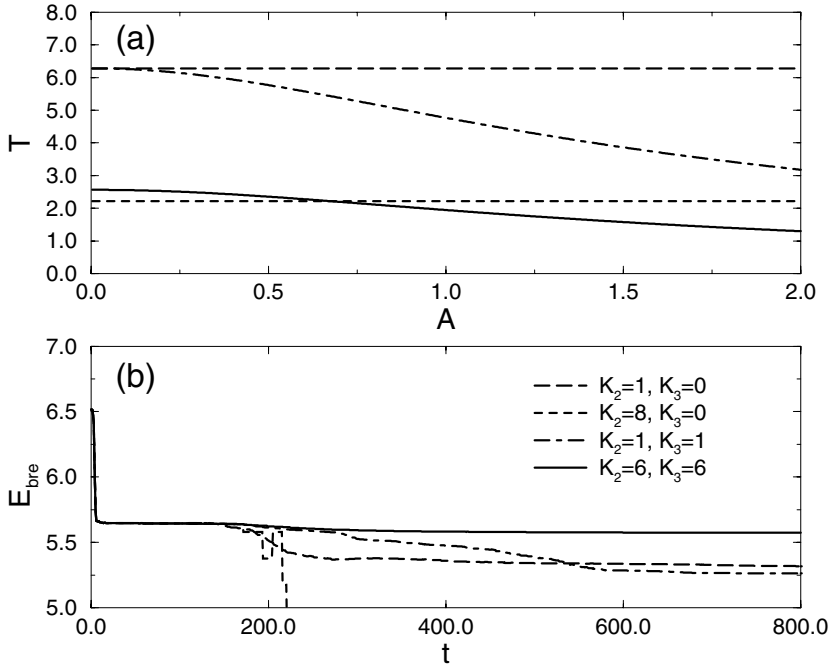

Figure 3. (*a*) Period of oscillation T for a single local potential V_p in (2), as a function of the initial amplitude $A(T_b \approx 2.1223)$. (*b*) Evolution of the energy of the breather defined as the sum of the local energy for the ± 4 sites around $n_{\max}$, where $n_{\max}$ is, in turn, defined as the site with largest local energy in the chain, viz. the centre of the breather. In these simulations $N_c = 51$. At $t \sim 170$, the breather enters into the curved region.

perpendicular direction, so that the energy loss is less dramatic. An exhaustive exploration in the parameter space (K_2, K_3) reveals that, in general, the breather adapts better to anharmonic potentials since the resonance is nonlinear. The breather dynamics of the three cases where the breather traverses the hairpin will be compared below.

Regarding the specifics of the DB propagation properties in the chain, we find that for a given injection velocity λ, there exists a critical curvature that determines whether the breather traverses the curved part of the hairpin. For the optimum case in figure 3(*b*), $K_2 = K_3 = 6$ and the velocity parameter $\lambda = 0.8$, we plot in figure 4 the evolution of the breather for different curvatures. We find that for large enough curvatures (small N_c), the breather cannot enter completely in the curved region of the hairpin and it either rebounces or gets trapped in the bend while for smaller curvatures, the breather traverses efficiently through the bend. The critical penetration curvature depends on the initial DB velocity as in reference [18] and also on the specifics of the perpendicular potential.

In order to understand the nature of the exchange between the two local orthogonal directions, we focus on the local DB motion for three of the cases shown in figure 3(*b*). In figure 5 we show the breather motion in the curved part of the chain for the angular coordinate. Note here that when showing the motion in the curved part of the chain we use (absolute) polar coordinates, σ_n for the angular or longitudinal motion and r_n for the radial or perpendicular dynamics (see figure 1(*b*)). The longitudinal chain motion shown in figure 5 is similar in all three cases and correponds predominantly to the x-motion for the breather in the straight part of the chain. Due to the small energy loss, the period of the breather (hence, the period in the

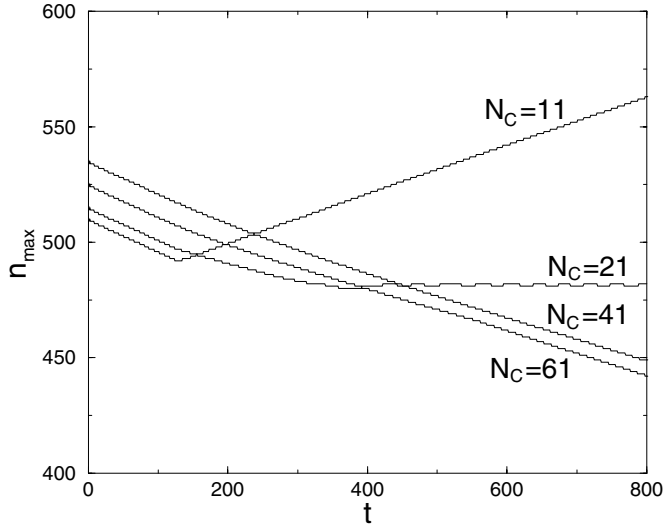

Figure 4. Fixing $K_2 = 6$, $K_3 = 6$ for V_p and $\lambda = 0.8$ for the translational velocity of the breather, we vary the curvature of the hairpin with N_c. We show the position of the breather $n_{\max}$ at every time. At $t \sim 170$, the breather arrives at the curved region in all cases.

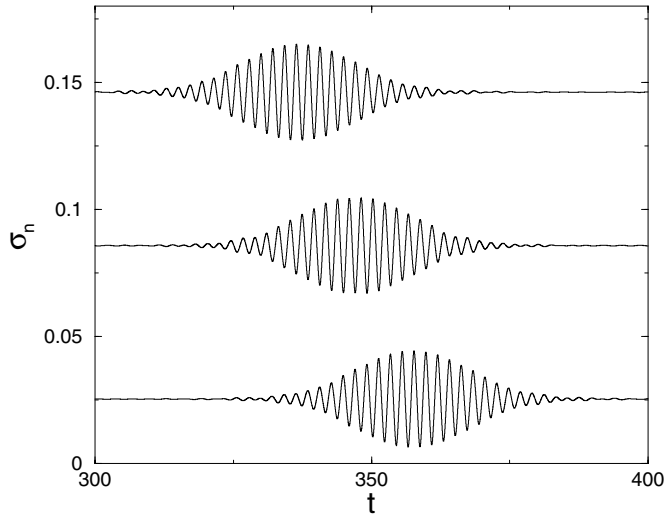

Figure 5. Angular coordinate, σ_n, for the breather in the curved part of the hairpin. The three central sites located at point 2 in figure 1 are shown, although for different time windows, this figure applies to the three cases in figure 6.

oscillations in figure 5) are slightly larger than T_b; we note that in the worst case this difference reaches only the 2% level. The transverse component of the DB motion in the curve is presented in figure 6 for three of the cases shown in figure 3. For the parameters of figure 6(a), $K_2 = 1$ and $K_3 = 0$, we note that in this far-from-resonance case, the transverse breather

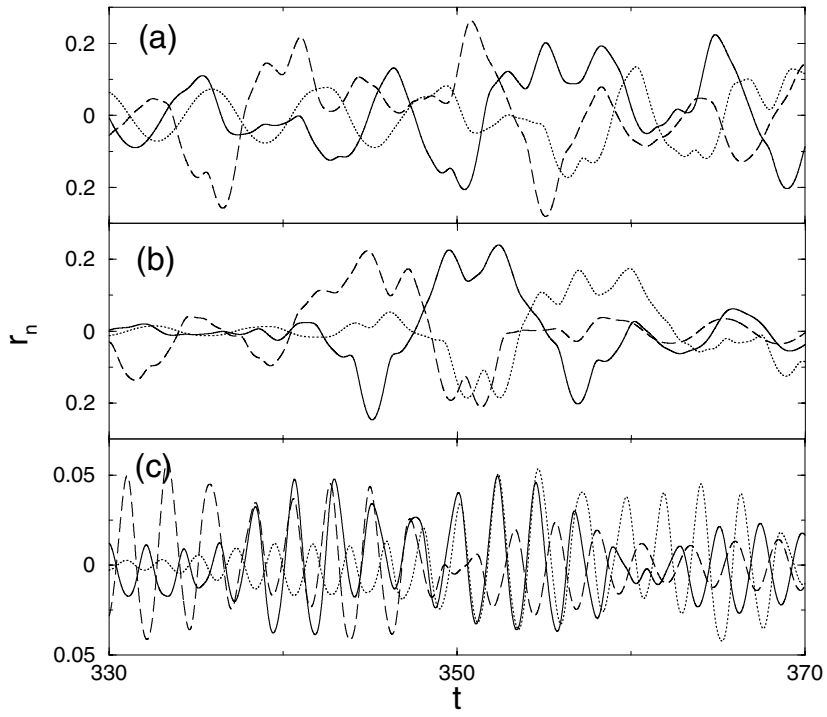

Figure 6. Dynamics, in radial coordinates, r_n, of the breather motion in the centre of the curve. (*a*) Case with $K_2 = 1$ and $K_3 = 0$. (*b*) Case with $K_2 = 1$ and $K_3 = 1$. (*c*) Case with $K_2 = 6$ and $K_3 = 6$. Note how only case (*c*) shows a coherent periodic motion with the same T_b for radial coordinates. In all the panels, the central particle of the hairpin (at point 2 in figure 1) is shown (solid curve), as well as the previous (dashed curve) and the following (dotted curve) nodes.

coordinates oscillate neither coherently nor with a period similar to the longitudinal one. Although the majority of the breather energy is transmitted coherently longitudinally, the fact that the perpendicular motion is aperiodic inhibits the efficiency of the propagation through the bend and augments the energy loss. We observe similar behaviour in figure 6(*b*) for the second set of parameters, although the perpendicular motion is, in this case, more coherent as a result of the nonlinear nature of the potential and the subsequent induction of oscillations at different frequencies. The most resonant situation is shown in figure 6(*c*). This potential enables coherent radial oscillations that minimize DB energy losses and favours the motion of the breather through the bend. This resonant motion affected through the geometrical coupling between two orthogonal DB directions is a direct consequence of the good matching between the period of the induced oscillation in the perpendicular potential and the breather period T_b shown in figure 3(*a*).

We note that the combined oscillation in the longitudinal (figure 5) and radial (figure 6(*c*)) directions constitutes a two-dimensional breather that originates from the initial one-dimensional FPU breather and came into existence as a result of the geometrical–dynamical coupling between two perpendicular directions. We point out that the longitudinal motion dominates the transverse motion, so the breather could be considered as a quasi-one-dimensional with a small orthogonal component. In figure 7 we present a snapshot of the breather as it reaches point 2 of figure 1. In order to compare with figure 2(*a*) we have plotted relative polar coordinates, $\zeta_n \equiv \sigma_n - \sigma_{n-1} - \alpha$, where α is the equilibrium angle for two

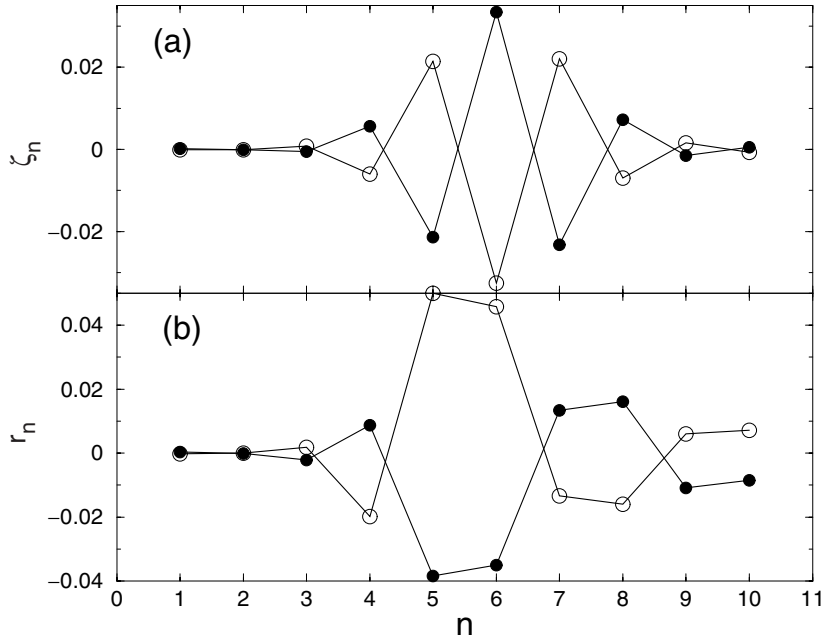

Figure 7. (*a*) Relative angular coordinate, ζ_n, for the breather when it reaches point 2 of the hairpin. (*b*) Radial coordinates for the breather at that point. The different curves correspond to the beginning of the period (filled circles) and after $T_b/2$ (empty circles) for the resonant case in figure 6(*c*).

consecutive sites in the curve. By doing so, ρ_n and ζ_n in figures 2(*a*) and 7(*a*), respectively, are directly comparable. We note that the breather in the bend region, while continuing having a longitudinal shape similar to the initial one, forms a multibreather in the radial direction. As a result, this two-dimensional localized object moves efficiently in the bend with a complex structure dictated by symmetry and energy reasons.

The adaptive feature of the 2D breather shown in figure 6(*c*) is more clearly observed in figure 8. The efficient coupling between angular and radial motion for this case allows the breather to adapt its orientation after some ($\approx$4) oscillations before passing from one site to the next one in the chain.

Finally, the breather, after traversing the bend region, re-enters in the second rectilinear segment of the hairpin; the local geometry once again forces the DB to adapt to the new environment. As a result, the breather evolves and transforms its vertical multibreather structure into longitudinal motion, while shedding away miniscule amounts of energy that are minimal in the most resonant case. The final shape of the breather is almost the same as that of the one before entering the curve shown in figure 2.

4. Effect of low temperatures and dissipation

The stability of the breathers presented in previous sections is now tested against thermal fluctuations. In order to connect the chain to a heat bath at temperature T we use the Langevin prescription for each lattice site, even though other approaches might be more useful in biological applications [6]; the equations of motion resulting from equations (1)–(3) are

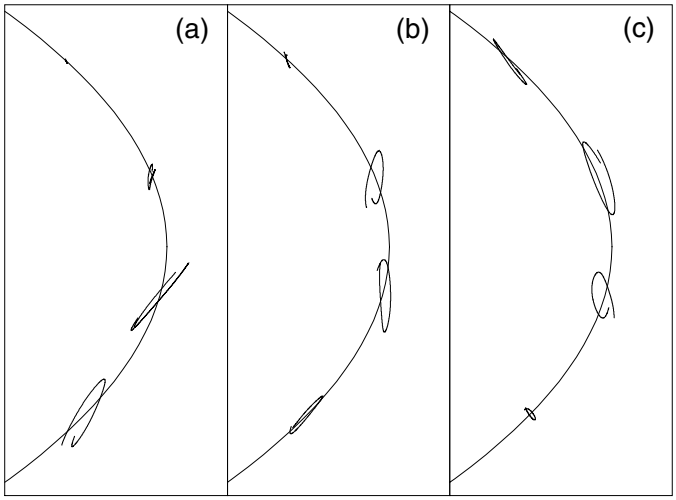

Figure 8. One-period (T_b) motion of the three central sites of the hairpin when the breather reaches these positions. (*a*) The breather is entering the central site from below with the orientation of the curve of the first site at the bottom. (*b*) After four periods T_b the breather is now in the central site and has adapted its orientation. (*c*) After four more periods, the breather is passing the third site (above) with a new adapted orientation. The continuous curve is the equilibrium line of the particles.

further modified by the inclusion of a fluctuating contribution and a damping term, leading to

$$\begin{aligned} \ddot{x}_n &= -\frac{\partial}{\partial x_n}\left[V_d(d_n) + V_p(r_n)\right] - \gamma \dot{x}_n + \eta_n^x(t) \\ \ddot{y}_n &= -\frac{\partial}{\partial y_n}\left[V_d(d_n) + V_p(r_n)\right] - \gamma \dot{y}_n + \eta_n^y(t). \end{aligned} \tag{6}$$

The $\eta_n^i(t)$ are mutually uncorrelated zero-centred Gaussian δ-correlated fluctuations that satisfy the fluctuation–dissipation relation

$$\left\langle \eta_n^i(t)\eta_m^j(t')\right\rangle = 2\gamma k_B T \delta_{ij}\delta_{nm}\delta(t-t') \tag{7}$$

for both coordinates $(i, j) = (x, y)$.

Discrete breathers do not survive to strong dissipation or noise and decay quite rapidly. On the contrary, for small damping and temperature, DBs show a strong resistance to decay as a result of the presence of the thermal bath. When DBs are compared with other nonstationary lattice fluctuations induced by the noise, they show a very slow energy decay and a rather good conservation of their integrity even after long times. In order to make these statements more quantitative, we address numerically dynamical properties of the two-dimensional DBs appearing in the curved part of our nonlinear chains. Implementation of damping and noise in equation (6) has to be solved using the second-order Runge–Kutta method.

In figure 9 we present numerical results of the resonant hairpin case shown in figure 6(*c*), with the presence of weak noise and damping ($T = 0.0001$ and $\gamma = 0.001$). DBs also exhibit in this geometry a particular resistance to be destroyed by the thermal bath and show slow decay yet retain their structure for a relatively long time. This resilience to decay is also present when the DB has also adapted to the curved geometry, as is evident from the long-dashed line in figure 9. The breather inside the hairpin shows similar structure and symmetry as shown in figure 7.

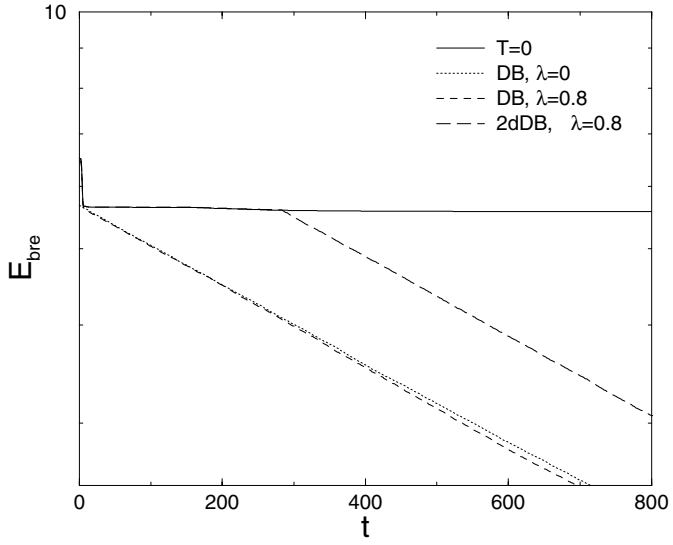

Figure 9. Energy of the localized structures (defined as E_{bre} in previous figures) for different cases. The solid line corresponds to the mobile DB without heat bath (the same solid case in figure 3(*b*)). The dotted line stands for the case with the DB in the straight part of the hairpin without translational motion ($\lambda = 0$). The case of a mobile DB is shown as a dashed line. For the long-dashed line, we enable the temperature once the DB has already entered the curve of the hairpin (when the straight line breaks). In all the cases the parameters of the bath are $T = 0.0001$ and $\gamma = 0.001$.

An analysis of the simulation data also indicates that the breather period grows and its amplitude decreases as a function of time. Moreover, if the breather is moving we observe a reduction of its translational velocity. By increasing noise and damping these effects are enhanced in such a way that the breather loses its internal coherent motion and symmetry and can be destroyed. A more detailed study of this phenomenology will be presented elsewhere [19].

5. Conclusions

Discrete breathers are nonlinear impurity modes in discrete lattices that are generally stable and in many cases mobile. In elastic polymer-like chains that extend on the plane, DB dynamical features are more complex. Presently, we use a standard FPU chain with nearest-neighbour interactions augmented with onsite potentials placed in direction perpendicular to the chain in order to study DB elastic and kinetic properties for a hairpin planar chain geometry. We found that DBs propagate efficiently through the bend, especially when the longitudinal DB frequency can resonate with perpendicularly placed onsite potential. This near resonance improves in the presence of nonlinear terms in the perpendicular potential. In all cases some DB energy loss is observed that increases in the less resonant cases. The motion is governed by the local energy conservation of breather internal and translational motion. The breather is seen to adapt to the local dynamical environment through small frequency shifts and velocity alteration while inducing motion in the perpendicular direction. When a near resonance can be induced with onsite nonlinear force field, the resulting two-dimensional breather moves very efficiently through the curved region, while upon re-entering the straight segment it recovers the one-dimensional properties. When thermal fluctuations and small damping are added in

the system, the DB propagation remains similar but a very slow, yet discernible energy loss is evident resulting finally in the DB decay. These DB features in polymer-like chains suggest that the breathers are efficient energy transporters in bend polymer chains since they can adapt to local changes and propagate with minimal distortion.

Acknowledgments

This work has been supported by the European Union under the RTN project LOCNET (HPRN-CT-1999-00163) and by the Dirección General de Enseñanza Superior e Investigación Científica (Spain) under projects SAB1999-0059, BXX-1001 and BFM2000-0624.

References

[1] Sievers A J and Takeno S 1988 *Phys. Rev. Lett.* **61** 970
[2] Bickham S R, Kiselev S A and Sievers A J 1993 *Phys. Rev.* B **47** 14206
[3] Aubry S 1996 *Physica* D **103** 201
[4] Marin J L and Aubry S 1996 *Nonlinearity* **9** 1501
[5] Chen Ding, Aubry S and Tsironis G P 1996 *Phys. Rev. Lett.* **77** 4776
[6] Tsironis G P and Aubry S 1996 *Phys. Rev. Lett.* **77** 5225
[7] Flach S and Willis C R 1998 *Phys. Rep.* **295** 182
[8] Rasmussen K O, Aubry S, Bishop A R and Tsironis G P 2000 *Eur. J. Phys.* B **15** 169
[9] Aubry S, Kopidakis G, Morgante A M and Tsironis G P 2001 *Physica* B **296** 222
[10] Swanson B I *et al* 1999 *Phys. Rev. Lett.* **82** 3288
[11] Binder P *et al* 2000 *Phys. Rev. Lett.* **84** 745
[12] Trias E, Mazo J J and Orlando T P 2000 *Phys. Rev. Lett.* **84** 741
[13] Xie A, Van der Meer L, Hoff W and Austin R H 2000 *Phys. Rev. Lett.* **84** 5435
[14] Kopidakis G, Aubry S and Tsironis G P *Phys. Rev. Lett.* at press
[15] Lomdahl P S, Olsen O H and Samuelsen M R 1991 *Phys. Lett.* A **152** 343
[16] Zolotaruyk A V, Christiansen P L and Savin A V 1996 *Phys. Rev.* E **54** 3881
[17] Gaididei Yu B, Mingaleev S F and Christiansen P L 2000 *Phys. Rev.* E **62** R53
[18] Tsironis G P, Ibañes M and Sancho J M Transport of localized vibrational energy in biopolymer models with rigidity *Preprint* (LOCNET database www.ma.hw.ac.uk/LOCNET/publications.html)
[19] Reigada R, Tsironis G P, Ibañes M and Sancho J M, in preparation